ACS NANO

www.acsnano.org

ARTICLE

Assembly of Polymer-Grafted Nanoparticles in Polymer Matrices

Clement Koh, Gary S. Grest, and Sanat K. Kumar*

Cite This: *ACS Nano* 2020, 14, 13491−13499

Read Online

ACCESS | Metrics & More | Article Recommendations

ABSTRACT: **Leibler pioneered the idea that long enough matrix polymers of length P will spontaneously dewet a chemically identical polymer layer, comprising chains of length N, densely end-grafted to a flat surface ("brush"). This entropically driven idea is routinely used to explain experiments in which 10−20 nm diameter nanoparticles (NPs) densely grafted with polymer chains are found to phase separate from chemically identical melts for $P/N \gtrsim 4$. At lower grafting densities, these effects are also thought to underpin the self-assembly of grafted NPs into a variety of structures. To explore the validity of this picture, we conducted large-scale molecular dynamics simulations of grafted NPs in a chemically identical polymer melt. For the NPs we consider, in the ≈5 nm diameter range, we find no phase separation even for $P/N = 10$ in the absence of attractions. Instead, we find behavior that more closely parallels experiments when all of the chain monomers are equally attractive to each other but repel the NPs. Our results thus imply that experimental situations investigated to date are dominated by the surfactancy of the NPs, which is driven by the chemical mismatch between the inorganic core and the organic ligands (the graft and free chains are chemically identical). Entropic effects, that is, the translational entropy of the NPs and the matrix, the entropy of mixing of the grafts and the matrix, and the conformational entropy of the chains appear to thus have a second-order effect even in the context of these model systems.**

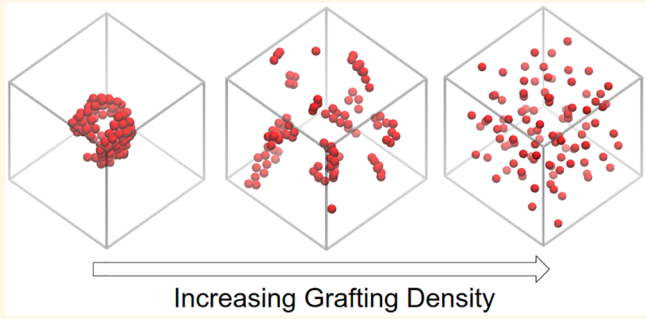

KEYWORDS: *grafted nanoparticles, autophobic dewetting, entropic effects, surfactancy, self-assembly, phase behavior*

Adding nanoparticles (NPs) can significantly impact the thermomechanical, optical, and electrical properties of a polymer melt. The control of NP morphology, that is, their spatial dispersion within the polymer matrix, is essential to optimizing these desired properties. The major complication in these contexts is that most NPs are inorganic and hence hydrophilic; in contrast, most polymers are hydrophobic. These systems, which are thus akin to oil−water mixtures, are generally incompatible. There are several methods that have been developed to address this issue and hence tune NP dispersion—here, we focus on one popular method where polymer chains are chemically grafted to the NP surface. Frequently, these chains have the same chemistry as the matrix polymer to which the NPs are added. The control variables in this context include the grafting density of the polymer chains on the NP, Σ, the ratio of the matrix chain length, P, to graft chain length, N, the NP diameter, D, and the volume fraction of the grafted NP, ϕ_{NP}.

A central concept in this area is the entropically driven autophobic dewetting of the brush chains by the matrix, even when they are of the same chemical structure but can be of different length.[2] While mixing entropy favors the interpenetration of free (matrix) chains into the grafted layer, this is opposed by chain stretching for both species. For sufficiently long matrix chains, the stretching dominates and the matrix "autophobically" dewets the brush. Such entropically driven effects have been demonstrated both experimentally and theoretically (both using analytical methods and computer simulations) in the limit of zero curvature (*i.e.*, flat surfaces).[3] The dewetting of the brush by the matrix chains implies that the spreading parameter, defined as $S = \gamma_{sv} - \gamma_{lv} - \gamma_{sl} \leq 0$. Here γ_{sv}, γ_{lv}, and γ_{sl} are the surface tension of the brush, the melt, and the interfacial tension between the brush and the melt, respectively. Under the reasonable approximation $\gamma_{sv} \approx \gamma_{lv}$, it follows that the dewetting of a polymer droplet on the brush

Received: July 2, 2020
Accepted: October 1, 2020
Published: October 8, 2020

https://dx.doi.org/10.1021/acsnano.0c05495
ACS Nano 2020, 14, 13491−13499

can only occur when $\gamma_{sl} > 0$. As this implies that the brush and the matrix are thermodynamically immiscible, it is commonly accepted that autophobic dewetting and miscibility are terms that can be used interchangeably.

Given this background, there is therefore reason to believe that the autophobic dewetting mechanism should also operate for large (*e.g.*, 100 nm diameter) spherical grafted NPs. Indeed, for NPs larger than ≈10 nm, it has been found experimentally that phase separation occurs for $P/N \gtrsim 4$ for NPs densely grafted with polymer chains. The experimental situation for NPs in the smaller size (*i.e.*, in the 2−5 nm) range is more complex. In addition to the autophobic dewetting phenomenom discussed above, two other factors appear to be relevant. First, for small enough NPs, the translational entropy of the NPs becomes important, and in this case, miscibility between the NPs and the polymer becomes easier. Also important is the role of energetic effects, in particular, the realization that bare NPs (without polymeric tethers) often phase separate from the matrix polymers. Thus, the key factors are the relative interaction strengths between two chain monomers, a monomer with the NPs and between two NPs (appropriately scaled to account for size differences). This latter effect, which leads to NP surfactancy, is expected to dominate at low grafting densities where both the surface and the graft chains can interact with the matrix chains. The major outstanding question then is the relative importance of the surfactancy of the NPs (enthalpic effects) *versus* entropic effects in determining the phase and self-assembly behavior of this class of systems.

This topic has been the focus of many theoretical and simulation studies.[1,4−17] A noncomprehensive search of the literature reveals over 800 papers on this subject, including several from our groups. However, as we shall elaborate below, there is no clear, unequivocal theoretical understanding of these questions. Most work to date has been on single grafted NPs in a polymer matrix of the same chemistry.[2,18−27] No signatures of autophobic dewetting were found across the broad spectrum of Σ, N, and P values studied. These single-NP simulations are thus inconclusive in terms of our understanding. Perhaps more relevant are studies of the potential of mean force (PMF) between two polymer-grafted NPs in a polymer matrix, where the graft and matrix chains are chemically identical.[18,21,28−31] Interestingly, it was found that the PMF between two NPs went from being repulsive everywhere for $P/N = 1$ to having an attractive well for $P/N = 7$.[21] Three points are pertinent. First, the $N = 10$ value used in these simulations is too short to be considered polymeric. Second, it is unclear if the attractive well in the PMF between two NPs for $P/N = 7$ is sufficient to yield phase separation and/or self-assembly. Finally, the grafting density values used Σ = 0.38 or 0.76 (in units of chains/σ^2) are too large to explicitly allow us to consider the role of surfactancy and how it interacts with the entropic effects of interest. There have also been simulations using multiple NPs.[32−41] Whereas the works of Liu *et al.*[39] and Shen *et al.*[35] are closest in spirit to experiments, that is, where the grafts and matrices are of the same chemistry, they were restricted to relatively short grafts ($N = 10$) in one case, whereas in the latter, only limited ranges of P/N were explored for longer $N = 30$ grafts. Although many other studies have considered longer grafts and a broader range of P/N, these are when the graft and matrix chains are not identical. There is therefore a paucity of well-established benchmark simulations where grafted polymers are identical in chemistry with the matrix. This is precisely the focus of the current study.

A final point to be emphasized here is how we separate and study purely entropic, autophobic dewetting, effects. Previous work[42] in the somewhat unrelated context of the miscibility of hydrocarbons, that is, polyethylene (PE) and polypropylene (PP), has important points that we re-emphasize here and learn from. PE and PP are made of the same constituents, $-CH_x-$, with the difference being their connectivity. The simplest model, which is purely entropic in origin, is to consider chains with these different microstructures and how their different local packings yield unfavorable entropies. This simple packing-based model, which has only repulsive interactions and ignores any attractions, suggests that such entropic effects, though present and unfavorable, are not large enough to cause phase separation. In contrast, when attractive interactions, which are equal across both species, are introduced then phase separation occurs.

Conclusively deciding on the role of entropy thus requires us to consider purely repulsive systems because, otherwise, the effects observed could represent a coupling of packing and energetics. In our work, we perform the first comprehensive simulation study of the miscibility of multiple NPs grafted with polymeric tethers as long as $N = 100$ in matrices that are long enough (*i.e.*, $P/N \leq 80$) to critically examine the role of autophobic dewetting in determining the phase behavior of these materials. We find no such phase separation for completely repulsive systems, likely due to the small sizes of the NP used ($D = 5\sigma$, where σ is the monomer size). Instead, we find behavior that closely matches experimental trends when attractions are introduced between all species, except between the NPs and the chains, which remains repulsive. Our results therefore emphasize the importance of enthalpic effects in determining and understanding the self-assembly and phase behavior of this important class of materials.

RESULTS AND DISCUSSION

Past works, which do not directly address the phenomenon of autophobic dewetting, motivate the current work where we simulate systems containing 100 NPs. Although we are primarily interested in completely repulsive systems where entropic effects dominate, we also systematically vary interactions to be attractive across the three different pairs of species (namely, NP−NP, NP−polymer, and polymer−polymer) with the constraint that the matrix and graft are always of identical chemistry.

Whereas details of our simulations are in the Methods section, we sketch some essential aspects here. We simulate grafted NPs with a diameter of $D = 5\sigma$ (where σ is the size of a chain monomer) at various ϕ_{NP} (mainly 0.015, with some at 0.022); the NPs are uniformly tethered with bead−spring polymer chains with length $N = 10$, 40, or 100. The graft points are rigidly fixed to the NP surface. The matrix consists of bead−spring chains of fixed length in the range $P = 6−800$. In this paper, we focus on systems with $N = 40$ (specifically the symbols with circles in Figure 1), whereas the other N and P values in Figure 1, which yield qualitatively similar results, are mainly deferred to future publications. We model both flexible chains ($k_\theta = 0$) and stiffer chains with bending stiffness ($k_\theta = 1.5\epsilon$): in each case, the grafts and the matrix chains are of the same stiffness. The interactions between nonbonded monomers (graft−graft, graft−matrix, and matrix−matrix) are described by the Lennard-Jones potential. However, in one

https://dx.doi.org/10.1021/acsnano.0c05495
ACS Nano 2020, 14, 13491−13499

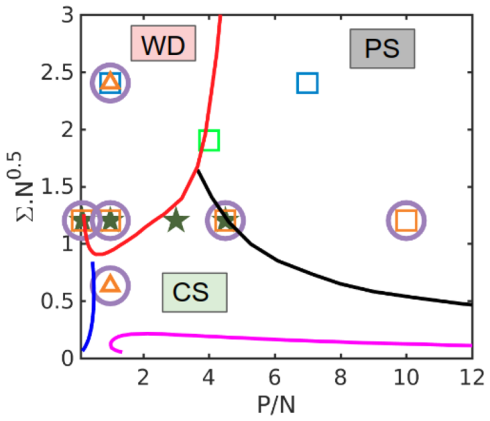

Figure 1. Composite morphology diagram with approximate boundaries (lines) derived from experimental data.[1] We only show three morphologies: well-dispersed (WD), phase separated (PS), and connected sheets (CS). The diagram is overlaid with simulation data points for a range of N = 10−100 and P = 6−400, and Σ = 0.1−0.76. The blue squares are for the N = 10, Σ = 0.76, and $k_\theta = 1.5\epsilon$ systems. The green square is for a N = 100, Σ = 0.19, and $k_\theta = 1.5\epsilon$. The green stars are for the N = 40, Σ = 0.19, and k_θ = 0 systems. The orange squares are for the N = 40, Σ = 0.19, and $k_\theta = 1.5\epsilon$ systems. The orange triangles correspond to N = 40, P = 40 but with Σ varying from 0.1 to 0.38 ($k_\theta = 1.5\epsilon$). The points circled in purple (ϕ_{NP} = 0.015) are the main focus of this paper.

case, we employ a purely repulsive interaction by truncating the potential at $r_c = 2^{1/6}\sigma$, whereas in the attractive case, r_c = 2.5σ. The interactions between a NP and a monomer and between two chain monomers (and NP−NP) are independently varied to be attractive or repulsive depending on the system simulated (see below). By varying N, P, and Σ, we probed a design space significantly more extensive than experimentally accessed (Figure 1).

We explicitly simulate three cases. In the *repulsive* system, all interactions are truncated at the minimum, that is, $r_c = 2^{1/6}\sigma$, so that there is no attraction across the different pairs. Similarly, in the *attractive* case, all interactions are truncated at r_c = 2.5σ. The choice of these two cases is inspired by previous work on hydrocarbon-based polymers discussed above. Finally, in the *partially* attractive case, the interactions between any pairs of chain monomers and between two NPs are truncated at r_c = 2.5σ, so that they have attractions, whereas the interaction between a chain monomer and a NP is truncated at $r_c = 2^{1/6}\sigma$, so that it is repulsive. This last case allows us to systematically examine the role of surfactancy in these situations. One last methodological detail is the density condition simulated. In the case of a pure melt with attractive interactions simulated in the isothermal−isobaric ensemble with P = 0, we found that monomer density is $\rho\sigma^3 \approx 0.89$ (in the limit of long chains). We simulate the repulsive systems at this density in the NVT ensemble to facilitate direct comparisons to the attractive systems.

Repulsive Systems. We first focus on the semiflexible chain system ($k_\theta = 1.5\epsilon$) in which all pair interactions are purely repulsive. Figure 2a−d corresponds to Σ = 0.19, N = 40, and P = 400 (square with a purple circle in Figure 1). Simulation snapshots provide a quick summary of the temporally evolving NP dispersion state, and Figure 2d shows that the grafted NPs are completely dispersed. Figure 2g (inset) shows an essentially featureless, gas-like NP−NP

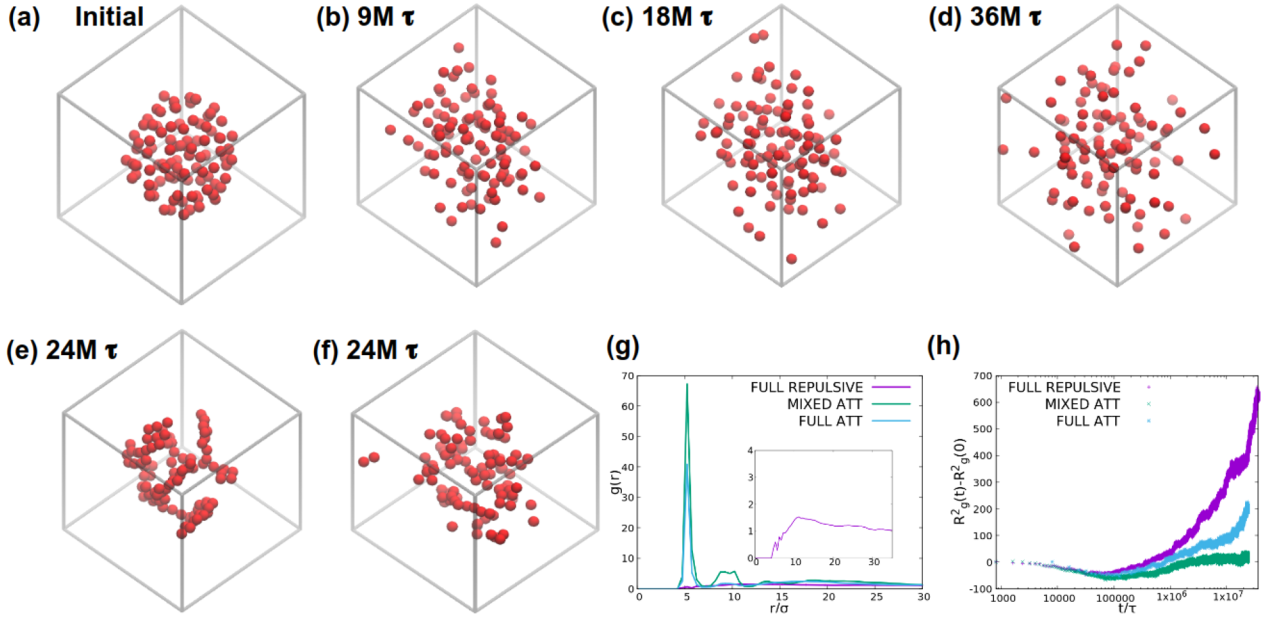

Figure 2. (a−d) Snapshots of the central simulation cell[43] for a system with 100 NPs with N = 40, Σ = 0.19, and P = 400 ($k_\theta = 1.5\epsilon$) at various simulation times with purely repulsive interactions (ϕ_{NP} = 0.015). Simulation times are noted in each image, where 1M τ corresponds to $10^6\tau$ ($\tau = \sqrt{\frac{m\sigma^2}{\epsilon}}$ is the time scale implied by the Lennard-Jones potential). (e) Snapshot for the N = 40, P = 400 system but with mixed attractions, namely, polymer−polymer and NP−NP interactions are attractive, whereas NP−chain monomer interactions are a truncated−shifted interaction with no attractions. (f) Snapshot for the N = 40, P = 400 system but with attractive interactions between all pairs. (g) NP−NP pair distribution functions, $g(r)$, averaged over the last 0.8Mτ for N = 40, P = 400 with different interactions. The inset presents an expanded view of the repulsive system $g(r)$. (h) Mean squared radius of gyration (R_g^2) of the ensemble of NPs as a function of time.

https://dx.doi.org/10.1021/acsnano.0c05495
ACS Nano 2020, 14, 13491−13499

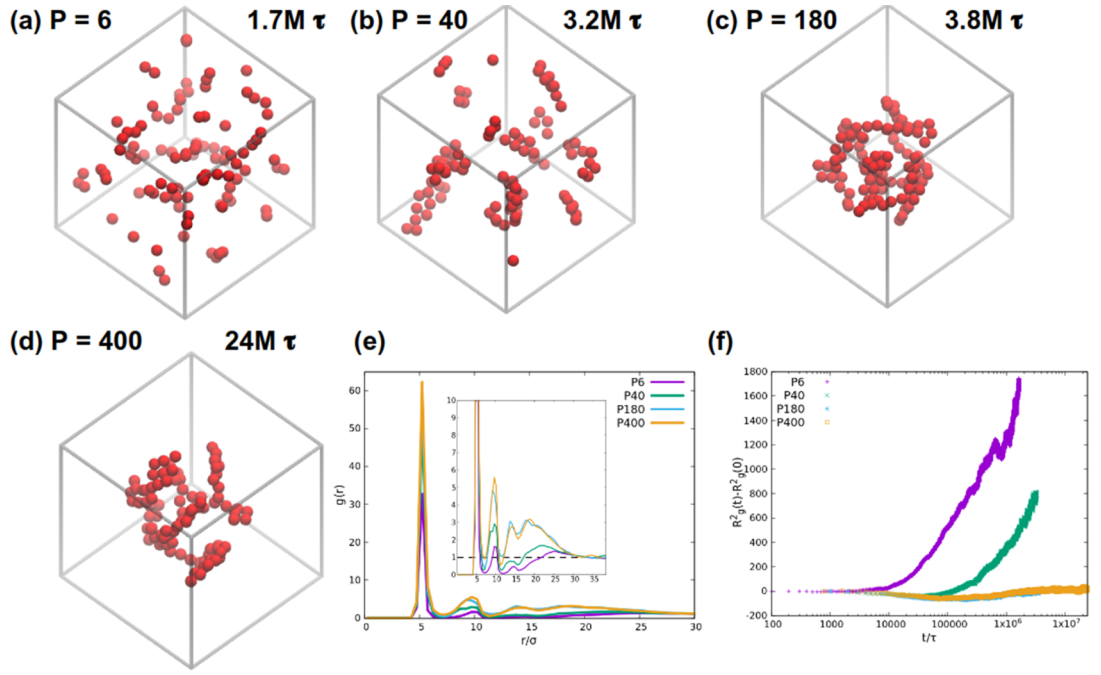

Figure 3. (a–d) Snapshots of simulation boxes for fixed $\Sigma = 0.19$, $N = 40$ with a range of $P = 6$ (a), 40 (b), 180 (c), and 400 (d) ($\phi_{NP} = 0.015$, $k_\theta = 1.5\epsilon$). Interactions are attractive for polymer–polymer and NP–NP but repulsive for polymer–NP. The simulation run times for each run are shown ($M\tau$ refers to $10^6\tau$). Polymer chains, both graft and matrix, are not shown for clarity. (e) NP–NP radial distribution functions, $g(r)$, for different P values averaged over the last $0.1M\tau$. The inset presents an expanded view. (f) Mean squared radius of gyration (R_g^2) of the ensemble of NPs as a function of time.

pair distribution function, $g(r)$, at the end of the long simulation, verifying this conclusion. Note that the simulation times in Figure 2d are roughly twice as long as the terminal time for a homopolymer melt with $P = 400$ ($1.9 \times 10^7\tau$; see Methods). Similar results were found for all of the cases we simulated (*i.e.*, all points in Figure 1). Further evidence that this purely repulsive system is dispersed is the mean square radius of gyration of the NPs, $R_g^2(t)$, which monotonically increases with time (Figure 2h). This implies that the NPs are moving in a diffusive manner and spreading out with time. Our essential result is that we do not have any evidence for an entropic phase separation in these systems with $D = 5\sigma$; this is particularly striking given this extreme case: $\Sigma = 0.19$, $N = 40$, and $P = 400$ has $P/N = 10$ at $\Sigma\sqrt{N} \approx 1.2$.

We thus verify that small enough NPs (in this case of $D = 5\sigma$), ones considerably bigger than the monomer size, do not experience phase behavior that is dominated by the reduced mixing between the matrix and brush chains. Rather, it appears that the translational entropy of the NPs and of the matrix chains dominate and lead to mixing under all the conditions we have simulated. We expect that, whereas smaller NPs will continue to display this same behavior where mixing entropy dominates, systems comprising larger NPs should show the expected entropically driven phase separation phenomenon. What the precise NP size where these autophobic dewetting effects dictate behavior is unclear, but these systems remain outside the purview of our current simulation abilities.

Systems with Attractions. To understand experiments, whose behavior is more closely represented by Figure 1, we have introduced attractions: both fully "attractive" and "partially attractive" cases are considered. Figure 2e–g illustrates some level of particle clustering in the fully attractive case (where all interactions are equally attractive) but much stronger clustering behavior for the partially attractive case (*i.e.*, all equally attractive, except NP–polymer interactions which are repulsive). There are differences, however: In the fully attractive systems, whereas the contact value of $g(r)$ is large, the radial distribution function is featureless for larger r. In contrast, partially attractive systems show much stronger structuring.

As seen in Figure 2h, the size of the NP "aggregate" does not change with time for the mixed attraction case, whereas it increases slowly with time for the fully attractive case. The results for the fully attractive systems are likely due to the NPs forming small stringy clusters which move slower than the well-dispersed NPs in the repulsive system. These small clusters are the origin of a strong first peak in $g(r)$ but with no features at larger r. The mixed attraction case forms a self-assembled structure which moves very slowly (if at all). The $g(r)$ in this case shows multiple peaks. This partially attractive case is thus very reminiscent of the previous work of Akcora *et al.*,[1,44] who suggested that the surfactant nature of the grafted NPs controlled the self-assembly and phase behavior seen in Figure 1.

We next explore this idea further and consider the partially attractive case across two systematic studies. Figure 3 considers systems at fixed $\Sigma = 0.19$, $N = 40$, while varying P from 6 to 400 ($k_\theta = 1.5\epsilon$); Figure 4 examines variations in Σ (from 0.1 to 0.38) for $N = 40$ and $P = 40$ ($k_\theta = 1.5\epsilon$). At fixed N and Σ, a horizontal line in Figure 1, we find that increasing P changes the NP morphology from well-dispersed ($P/N = 0.15$) to NP strings ($P/N = 1$) to the formation of larger self-assembled aggregates (possibly connected sheets) for the largest $P/N = 4.5$ and 10. The NP–NP radial distribution function in Figure 3e highlights the progressive immiscibility of the grafted NPs with increasing P/N, as illustrated by the higher values for all $g(r)$ peaks. Expanding on this point, Figure 3f shows that the P

https://dx.doi.org/10.1021/acsnano.0c05495
ACS Nano 2020, 14, 13491–13499

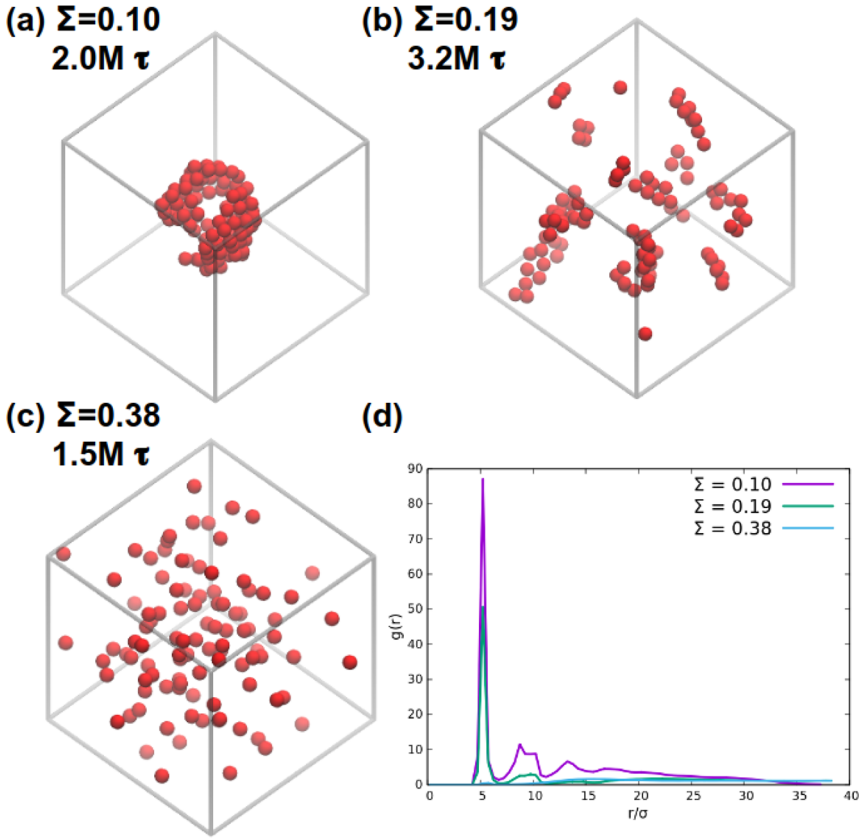

Figure 4. (a–c) Snapshots of the NPs for the $N = 40$, $P = 40$ system for $\Sigma = 0.1$, 0.19, and 0.38, respectively ($\phi_{NP} = 0.015$, $k_\theta = 1.5\epsilon$). Interactions are attractive for polymer–polymer and NP–NP but repulsive for polymer–NP. The simulation run times for each run are shown ($M\tau$ refers to $10^6\tau$). Polymer chains, both graft and matrix, are not shown for clarity. (d) Plot of the radial distribution function between two NPs, $g(r)$, averaged over the last $0.1M\tau$ for the three systems simulated here.

= 6 and $P = 40$ systems have considerable NP mobility, whereas the larger P systems are not dispersing. These results qualitatively agree with the experimental consensus that the transition between well-dispersed systems and phase-separated systems occurs at $P/N \approx 4$.

We also examined variations in Σ at fixed $N = P = 40$ (vertical line in Figure 1). As expected, Figure 4 shows that the system goes from an agglomerated state to one akin to strings and finally to well-dispersed NPs with increasing Σ. The low Σ system can be understood on the basis of the early work of Hooper and Schwezier[45] and Meng *et al.*,[46] who showed that, in the absence of an attractive interaction between the NP and the polymer, phase separation occurred due to depletion–attraction effects as embodied in the venerable work of Asakura and Oosawa.[47,48] This is also in agreement with the results deduced experimentally in Figure 1, which show that systems with smaller $\Sigma\sqrt{N}$ show particle clustering over a much broader range of P/N than the high $\Sigma\sqrt{N}$ systems where phase separation requires $P/N \gtrsim 4$.

To quantify the trends discussed above, we calculate the excess number of neighbors for a NP as follows: $N_{ex} \equiv S(0) = \int_0^\infty 2\pi r^2 \rho_{NP}[g(r) - 1]dr$, where ρ_{NP} is the NP number density and $S(0)$ is the zero wavevector limit of the static structure factor. Focusing on the data for the repulsive system in Figure 2, we find $N_{ex} < 1$ for both k_θ values for $\Sigma = 0.19$, $N = 40$, and $P = 400$. This implies minimal NP clustering, consistent with our conclusion that these entropically driven systems are miscible under all conditions we have simulated. In a similar vein, N_{ex} for the systems presented in Figure 3 increases as we go from $P/N = 0.15$ ($N_{ex} \approx 0$) to $P/N = 1$ ($N_{ex} \approx 5$) and finally $P/N = 4.5$ and 10 ($N_{ex} \approx 15$). Again, clustering is apparently only facilitated when we deal with mixed attractions, that is, when the surfactancy in the NPs is manifested explicitly.

Clearly, as experimental systems typically incorporate attractions, we conclude that the purely repulsive case does not serve as a good model for understanding the phase and the self-assembly behavior, especially for small NPs. Further, the different conclusions presented in the literature for $D = 5$ nm NPs must also be reflective of the energetics of the system studied (in that case with a gold core)[49−53] and not reflective of purely entropic effects. Interestingly, Corbierre *et al.*[54] observed predominantly dispersed gold NPs with only some aggregation for $P/N = 40$. We thus believe that the morphology diagram presented in Figure 1 is truly representative of the surfactant nature of the NPs, with these results apparently valid for the simulated NPs of $D = 5\sigma$. In contrast, the experimental systems from which these results are derived are in the $D \approx 5$–25 nm range. Hence, we believe that such morphology plots have broad ranges of applicability in the context of these NP systems.

We next comment on brush heights and how they are affected by P/N ratios. It has been shown experimentally for silica NPs grafted with polystyrene (PS) in a PS matrix that the brush height, h, collapses strongly when $P/N \gtrsim 4$.[55] Experimentally, the h was derived indirectly—the mean inter-NP spacing was deduced from X-ray or neutron scattering, d_s, and then $h \equiv (d_s - D)/2$.[55] For the simulation analogue of the experimental brush height metric, we took the

https://dx.doi.org/10.1021/acsnano.0c05495
ACS Nano 2020, 14, 13491−13499

position of the first peak in the inter-NP $g(r)$ and subtracted D and divided the whole quantity by 2.

In parallel, for the repulsive system with $N = 40$, $\Sigma = 0.19$ with varying P ($k_\theta = 0$), we computed $\langle h^\alpha \rangle = \frac{\int_D^\infty 4\pi r^2 \rho_g(r)(r-D)^\alpha dr}{\int_D^\infty 4\pi r^2 \rho_g(r)(r-D) dr}$, where $\rho_g(r)$ is the graft density for chains attached to the NP of interest. We have used both $\alpha = 1$ and 2, that is, both the first and second moment of the height distribution, and reported $\langle h^\alpha \rangle^{1/\alpha}$. All of these quantities are plotted in Figure 5a,b. The calculated brush heights using the density distributions from single-NP simulations and multi-NP simulations unsurprisingly give identical results for each α (*i.e.*, this follows from Figure 6). For small P/N, the results for $\alpha = 1$ approximately match those obtained from the experimental mimic. However, for larger P/N, we find that the real brush height calculated following the density distributions hardly changes with P, in good agreement with previous simulations.[20,21] It is important to note that while the real brush heights calculated from density profiles do not change much, there remains a small systematic decrease in brush height as P/N increases, as evident in Figure 5b. The experimental mimic, on the other hand, decreases by nearly 30%, qualitatively consistent with trends reported by Chevigny *et al.*[55] It is likely that the brush chains interpenetrate, with this degree of interpenetration increasing with P, giving rise to this experimental result, but the more important point is that this experimental measure does not properly characterize brush heights.

Finally, we note the relevance of our results of phase separation and self-assembly to experiments. In experimental systems, such as silica NPs grafted with PS in a PS matrix, the PS and the silica are immiscible as the PS−PS attractive interactions are much stronger than the PS−silica interactions. Parenthetically, we note that the silica NP−silica NP interaction is likely very much stronger than the PS−PS attraction. The fact that the simulations, which treat the NP−NP and monomer−monomer attractions to be equal in strength, can describe the experimental results in Figure 1, clearly show that the self-assembly phenomena are evidently not sensitive to such quantitative details.

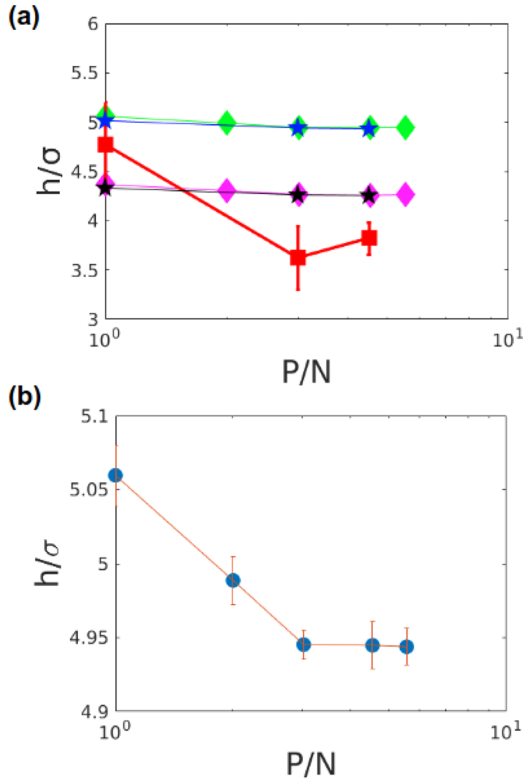

Figure 5. (a) Brush heights as a function of P/N for fully flexible chains ($k_\theta = 0$) for $N = 40$. The multi-NP systems are at $\phi_{NP} = 0.022$. The stars represent the brush heights for the multi-NP systems calculated *via* the first (black) and second (blue) moment of the graft densities. The diamonds represent the brush heights for the single-NP systems calculated *via* the first (magenta) and second (green) moments of the graft density distributions. The red squares represent the height derived from the NP−NP $g(r)$ values of the multi-NP systems. (b) Single-NP brush height as a function of the P/N ratio. P is varied while $N = 40$. A clear but subtle decrease in brush height is observed at larger P/N. Error bars are obtained by the block-averaging method. If error bars are absent, they are smaller than the symbols.

CONCLUSION

We clearly show that entropy by itself cannot explain the phase separation and self-assembly behavior of grafted NPs mixed with homopolymer chains of the same chemistry, especially when we consider small NPs (in this case of diameter $D \approx 5$ nm). We conjecture that chain packing frustration is reduced in curved brushes because of the increased available volume as one goes further away from the grafting surface. This relief, which is not available to the planar analogue, is favorable to mixing. Additionally, the relative contributions of the translational entropy of the NPs becomes larger with smaller NPs, and these two factors in combination apparently dominate the behavior of small grafted NPs. It is only through the introduction of (mixed) attractions that we were able to achieve the self-assembly (and phase separation) of the grafted NPs. In particular, with polymer−polymer and NP−NP attractions, but with a repulsive interaction between polymer−NP, we were able to observe the diverse self-assembled structures observed experimentally. These results thus verify our initial notion that the behavior of these NPs are dominated by their surfactant-like character.

METHODS

All polymer chains in our simulations are represented using the coarse-grained bead−spring model of Kremer and Grest.[56] All monomers have mass m and diameter σ. Nonbonded monomers separated by a distance r interact with a Lennard-Jones potential:

$$U_{i,j}(r) = \begin{cases} 4\epsilon\left[\left(\frac{\sigma}{r}\right)^{12} - \left(\frac{\sigma}{r}\right)^{6}\right] & r < r_c \\ 0 & r > r_c \end{cases} \quad (1)$$

where ϵ is the well depth and σ is the monomer size. A cutoff of $r_c = 2^{1/6}\sigma$ was used for the purely repulsive case, whereas $r_c = 2.5\sigma$ was used for the systems with attractions. The potential between connected monomers is defined by the finitely extensible nonlinear elastic potential with a spring constant $k = 30\epsilon/\sigma^2$ and a maximum bond extension parameter of $R_o = 1.5\sigma$. In addition, a three-body bending potential of the form $U_{bend} = k_\theta(1 + \cos\theta)$ is used to introduce stiffness to the polymer chains with $k_\theta = 0$ (flexible) or 1.5ϵ (stiff).

To model the pair interaction between the nanoparticles and polymer monomers, a shifted Lennard-Jones potential was used.

https://dx.doi.org/10.1021/acsnano.0c05495
ACS Nano 2020, 14, 13491−13499

$$U_{i,j}(r) = \begin{cases} 4\epsilon\left[\left(\frac{\sigma}{r-\Delta}\right)^{12} - \left(\frac{\sigma}{r-\Delta}\right)^{6}\right] & r < R_c \\ 0 & r > R_c \end{cases} \quad (2)$$

This form allows the potential interaction to be the same for all particles, independent of size. For NPs with a diameter of $D = 5\sigma$, $\Delta = 2\sigma$ for the interaction between a NP and a polymer monomer and $\Delta = 4\sigma$ for the interaction between two NPs. The cutoff radius is $R_c = r_c + \Delta$. For the repulsive interactions, $R_c = (2^{1/6} + 2)\sigma$, whereas for the attractive interactions, $R_c = (2.5 + 2)\sigma$.

The simulations are carried out using the Large Scale Atomic Molecular Massively Parallel Simulator (LAMMPS) software.[57] The multi-NP systems are initialized in two steps. First, the grafted NPs (matrix-free) are placed on a simple cubic lattice with the restriction that none of the monomers overlap the NPs. Overlaps between monomers are removed by performing an energy minimization of the system. The default minimization style in LAMMPS[57] (Polak-Ribiere version of the conjugate gradient algorithm) is used. The Lennard-Jones potential for the fully attractive case is then applied in a NVT ensemble simulation at $T = \epsilon/k_B$, and the system is allowed to evolve until a stable aggregated cluster of NPs is obtained. At this stage, the Nose-Hoover equations of motion are integrated with a time step $\delta t = 0.001\tau$, where $\tau = \sigma(m/\epsilon)^{1/2}$.

Separately, polymer melts are prepared following the procedure described by Auhl *et al.*[58] before indenting a spherical void in the center of the polymer matrix. The NP aggregate is then inserted in the void while maintaining its density at $\rho\sigma^3 = 0.89$ in a NVT simulation with time step $\delta t = 0.005\tau$. The systems with attractions were simulated at $P = 0.0$ in the NPT ensemble (Figure 2a). The temperature $T^* = k_BT/\epsilon = 1$. In addition to this choice of an initial configuration with aggregated NPs, we have separately performed several simulations with the NPs starting from the mixed state. The results in the two cases are qualitatively similar, but we use the former procedure in this paper to convincingly demonstrate that the dispersed NP state obtained for all repulsive systems is not a consequence of the initial dispersed NP state. Koski *et al.*[38] have also shown that it is more difficult for the NPs to reach an equilibrium macrophase-separated state than an equilibrium dispersed state.

When the systems are stable, they are then run at constant volume with a time step $\delta t = 0.008-0.01\tau$ using a Langevin thermostat with a damping time constant of 100τ to maintain temperature. The damping time constant is chosen so that it is weak enough to have no measurable effect on the dynamics of the system. For $P = 400$ systems, the simulations were run for up to 3.6 billion time steps. The number of monomers in our systems are related to the volume fraction of the NPs. Most of the simulations are at $\phi_{NP} = 0.015$. For the $N = 40$ systems with stiff chains, there are ≈380,000 chain monomers, and regardless of interaction type, the resulting simulation cell has dimensions of $L \approx 76.0\sigma$, with $\phi_{NP} = 0.015$. For the $N = 40$ systems with flexible chains, the final simulation cell has dimensions of $L \approx 66.0\sigma$, with $\phi_{NP} = 0.022$. The single $N = 100$ system has dimensions of $L \approx 81.0\sigma$, with $\phi_{NP} = 0.012$.

Figure 6 illustrates that the structure of the brush (as quantified by the brush density profile) is unaffected by the presence of additional NPs or of attractions. What is changed is the relative contribution of the matrix and the graft monomers from other NPs. It is evident that, while the single-NP calculation shows no effect of interactions, the matrix is the most depleted in the mixed attraction situation, followed by the full attraction and then the repulsive case. Clearly, in the case of mixed attraction, the matrix chains prefer to not contact the NPs. This drives more NP−NP interactions akin to what one might expect from depletion attraction.

To put the time scales for the results shown in Figure 2 into perspective, we measured the mobility of polymer chains in a homopolymer melt with 400 chains of length $P = 400$ (the longest free chain length we simulated) at density $\rho\sigma^3 = 0.89$ at $T^* = 1$. Results for the mean square displacement of the center of mass and the inner five monomers are shown in Figure 7 for $r_c = 2.5\sigma$. Using $g_1(t) = 3R_g^2$ as a criteria for determining the terminal diffusion time

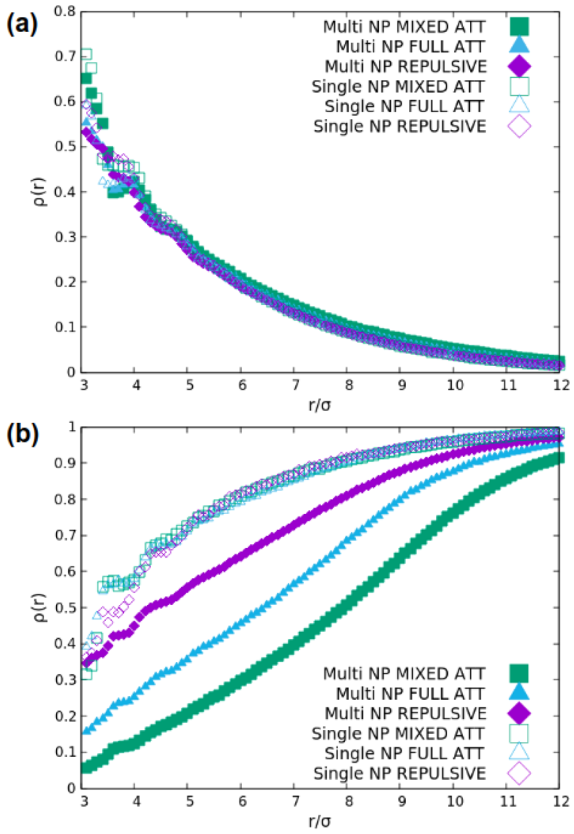

Figure 6. Density profiles for (a) graft monomers from the NP of interest and (b) of matrix monomers as a function of the distance from the center of the grafted NP for $N = 40$, $P = 400$ for the multiple NP system compared to a system with a single NP. The difference of the sum of these two quantities from 1 represents the contribution of brushes from other NPs.

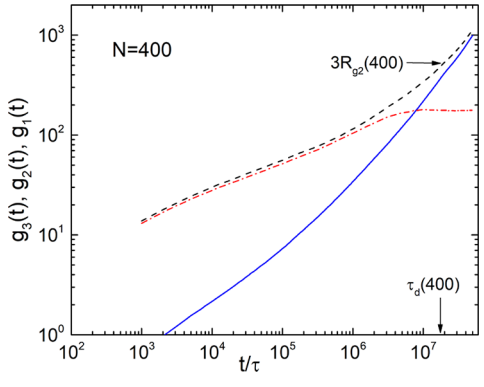

Figure 7. Simulations of melts of chains of length $P = 400$ with no NPs present. We plot the mean squared displacement of the center of mass $g_3(t)$ (blue solid line), inner five beads $g_1(t)$ (black dashed line), and motion of inner five bead relative to the center of mass $g_2(t)$ (red, dot-dash) lines for chains with $k_\theta = 1.5\epsilon$ for $r_c = 2.5\sigma$.

τ_d,[59] $\tau_d \approx 19M\tau$, which is less than the time scales we have run our $N = 40$, $P = 400$ systems. As found by Grest,[60] the terminal relaxation time for the pure repulsive case is essentially the same as for the attractive case for $T^* = 1$.

AUTHOR INFORMATION

Corresponding Author

Sanat K. Kumar − *Department of Chemical Engineering, Columbia University, New York, New York 10027, United*

https://dx.doi.org/10.1021/acsnano.0c05495
ACS Nano 2020, 14, 13491−13499

States; orcid.org/0000-0002-6690-2221; Email: sk2794@columbia.edu

Authors

Clement Koh − *Department of Chemical Engineering, Columbia University, New York, New York 10027, United States;* orcid.org/0000-0003-2214-1747

Gary S. Grest − *Sandia National Laboratories, Albuquerque, New Mexico 87185, United States;* orcid.org/0000-0002-5260-9788

Complete contact information is available at: https://pubs.acs.org/10.1021/acsnano.0c05495

Notes

The authors declare no competing financial interest.

ACKNOWLEDGMENTS

C.K. and S.K.K. thank the National Science Foundation (DMR-1709061) for funding this research. This research used resources at the National Energy Research Scientic Computing Center, which is supported by the Office of Science of the United States Department of Energy under Contract No. DE-AC02-05CH11231. These resources were obtained through the Advanced Scientic Computing Research (ASCR) Leadership Computing Challenge (ALCC). This work was performed, in part, at the Center for Integrated Nanotechnologies, an Office of Science User Facility operated for the U.S. Department of Energy (DOE) Office of Science. Sandia National Laboratories is a multimission laboratory managed and operated by National Technology and Engineering Solutions of Sandia, LLC, a wholly owned subsidiary of Honeywell International, Inc., for the U.S. Department of Energy's National Nuclear Security Administration under Contract No. DE-NA-0003525. C.K. and S.K.K. thank Ken Schweizer and Arthi Jayaraman for useful discussions on this paper.

REFERENCES

(1) Kumar, S. K.; Jouault, N.; Benicewicz, B.; Neely, T. Nanocomposites with Polymer Grafted Nanoparticles. *Macromolecules* **2013**, *46*, 3199−3214.
(2) Borukhov, I.; Leibler, L. Enthalpic Stabilization of Brush-Coated Particles in a Polymer Melt. *Macromolecules* **2002**, *35*, 5171−5182.
(3) Grest, G. S. Grafted Polymer Brushes in Polymeric Matrices. *J. Chem. Phys.* **1996**, *105*, 5532−5541.
(4) Pandey, Y. N.; Papakonstantopoulos, G. J.; Doxastakis, M. Polymer/Nanoparticle Interactions: Bridging the Gap. *Macromolecules* **2013**, *46*, 5097−5106.
(5) Vogiatzis, G. G.; Theodorou, D. N. Multiscale Molecular Simulations of Polymer-Matrix Nanocomposites. *Arch. of Comput. Methods Eng.* **2018**, *25*, 591−645.
(6) Ginzburg, V. V. In *Problems of Nonlinear Mechanics and Physics of Materials*; Andrianov, I. V., Manevich, A. I., Mikhlin, Y. V., Gendelman, O. V., Eds.; Springer International Publishing: Cham, Switzerland, 2019; pp 205−224.
(7) Hall, L. M.; Jayaraman, A.; Schweizer, K. S. Molecular Theories of Polymer Nanocomposites. *Curr. Opin. Solid State Mater. Sci.* **2010**, *14*, 38−48.
(8) Jayaraman, A.; Schweizer, K. S. Effective Interactions, Structure, and Phase Behavior of Lightly Tethered Nanoparticles in Polymer Melts. *Macromolecules* **2008**, *41*, 9430−9438.
(9) Jayaraman, A.; Schweizer, K. S. Structure and Assembly of Dense Solutions and Melts of Single Tethered Nanoparticles. *J. Chem. Phys.* **2008**, *128*, 164904.
(10) Jayaraman, A.; Schweizer, K. S. Effective Interactions and Self-Assembly of Hybrid Polymer Grafted Nanoparticles in a Homopolymer Matrix. *Macromolecules* **2009**, *42*, 8423−8434.
(11) Jayaraman, A.; Schweizer, K. S. Liquid State Theory of the Structure and Phase Behaviour of Polymer-Tethered Nanoparticles in Dense Suspensions, Melts and Nanocomposites. *Mol. Simul.* **2009**, *35*, 835−848.
(12) Chandran, S.; Begam, N.; Padmanabhan, V.; Basu, J. Confinement Enhances Dispersion in Nanoparticle−Polymer Blend Films. *Nat. Commun.* **2014**, *5*, 3697.
(13) Kulshreshtha, A.; Jayaraman, A. Dispersion and Aggregation of Polymer Grafted Particles in Polymer Nanocomposites Driven by the Hardness and Size of the Grafted Layer Tuned by Attractive Graft−Matrix Interactions. *Macromolecules* **2020**, *53*, 1302−1313.
(14) Harton, S. E.; Kumar, S. K. Mean-Field Theoretical Analysis of Brush-Coated Nanoparticle Dispersion in Polymer Matrices. *J. Polym. Sci., Part B: Polym. Phys.* **2008**, *46*, 351−358.
(15) Martin, T. B.; Jayaraman, A. Using Theory and Simulations to Calculate Effective Interactions in Polymer Nanocomposites with Polymer-Grafted Nanoparticles. *Macromolecules* **2016**, *49*, 9684−9692.
(16) Egorov, S. Interactions between Polymer Brushes in Solvents of Variable Quality: A Density Functional Theory Study. *J. Chem. Phys.* **2008**, *129*, 064901.
(17) Pryamtisyn, V.; Ganesan, V.; Panagiotopoulos, A. Z.; Liu, H.; Kumar, S. K. Modeling the Anisotropic Self-Assembly of Spherical Polymer-Grafted Nanoparticles. *J. Chem. Phys.* **2009**, *131*, 221102.
(18) Trombly, D. M.; Ganesan, V. Curvature Effects Upon Interactions of Polymer-Grafted Nanoparticles in Chemically Identical Polymer Matrices. *J. Chem. Phys.* **2010**, *133*, 154904.
(19) Lin, B.; Martin, T. B.; Jayaraman, A. Decreasing Polymer Flexibility Improves Wetting and Dispersion of Polymer-Grafted Particles in a Chemically Identical Polymer Matrix. *ACS Macro Lett.* **2014**, *3*, 628−632.
(20) Vogiatzis, G. G.; Theodorou, D. N. Structure of Polymer Layers Grafted to Nanoparticles in Silica−Polystyrene Nanocomposites. *Macromolecules* **2013**, *46*, 4670−4683.
(21) Meng, D.; Kumar, S. K.; Lane, J. M. D.; Grest, G. S. Effective Interactions Between Grafted Nanoparticles in a Polymer Matrix. *Soft Matter* **2012**, *8*, 5002−5010.
(22) Kalb, J.; Dukes, D.; Kumar, S. K.; Hoy, R. S.; Grest, G. S. End Grafted Polymer Nanoparticles in a Polymeric Matrix: Effect of Coverage and Curvature. *Soft Matter* **2011**, *7*, 1418−1425.
(23) Ndoro, T. V.; Voyiatzis, E.; Ghanbari, A.; Theodorou, D. N.; Böhm, M. C.; Müller-Plathe, F. Interface of Grafted and Ungrafted Silica Nanoparticles with a Polystyrene Matrix: Atomistic Molecular Dynamics Simulations. *Macromolecules* **2011**, *44*, 2316−2327.
(24) Ndoro, T. V.; Böhm, M. C.; Müller-Plathe, F. Interface and Interphase Dynamics of Polystyrene Chains Near Grafted and Ungrafted Silica Nanoparticles. *Macromolecules* **2012**, *45*, 171−179.
(25) Lo Verso, F.; Yelash, L.; Egorov, S. A.; Binder, K. Effect of the Solvent Quality on the Structural Rearrangement of Spherical Brushes: Coarse-Grained Models. *Soft Matter* **2012**, *8*, 4185−4196.
(26) Eslami, H.; Rahimi, M.; Müller-Plathe, F. Molecular Dynamics Simulation of a Silica Nanoparticle in Oligomeric Poly (Methyl Methacrylate): A Model System for Studying the Interphase Thickness in a Polymer−Nanocomposite *via* Different Properties. *Macromolecules* **2013**, *46*, 8680−8692.
(27) Klos, J.; Pakula, T. Computer Simulations of Chains End-Grafted onto a Spherical Surface. Effect of Matrix Polymer. *Macromolecules* **2004**, *37*, 8145−8151.
(28) Smith, G. D.; Bedrov, D. Dispersing Nanoparticles in a Polymer Matrix: Are Long, Dense Polymer Tethers Really Necessary? *Langmuir* **2009**, *25*, 11239−11243.
(29) Martin, T. B.; Dodd, P. M.; Jayaraman, A. Polydispersity for Tuning the Potential of Mean Force between Polymer Grafted Nanoparticles in a Polymer Matrix. *Phys. Rev. Lett.* **2013**, *110*, 018301.

(30) Munaò, G.; Correa, A.; Pizzirusso, A.; Milano, G. On the Calculation of the Potential of Mean Force between Atomistic Nanoparticles. *Eur. Phys. J. E: Soft Matter Biol. Phys.* **2018**, *41*, 38.
(31) Munaò, G.; Pizzirusso, A.; Kalogirou, A.; De Nicola, A.; Kawakatsu, T.; Müller-Plathe, F.; Milano, G. Molecular Structure and Multi-Body Potential of Mean Force in Silica-Polystyrene Nanocomposites. *Nanoscale* **2018**, *10*, 21656−21670.
(32) Yatsyshin, P.; Fytas, N. G.; Theodorakis, P. E. Mixing−Demixing Transition in Polymer-Grafted Spherical Nanoparticles. *Soft Matter* **2020**, *16*, 703.
(33) Koski, J. P.; Krook, N. M.; Ford, J.; Yahata, Y.; Ohno, K.; Murray, C. B.; Frischknecht, A. L.; Composto, R. J.; Riggleman, R. A. Phase Behavior of Grafted Polymer Nanocomposites from Field-Based Simulations. *Macromolecules* **2019**, *52*, 5110−5121.
(34) Martin, T. B.; Jayaraman, A. Tuning the Wetting−Dewetting and Dispersion−Aggregation Transitions in Polymer Nanocomposites Using Composition of Graft and Matrix Polymers. *Mater. Res. Express* **2016**, *3*, 034001.
(35) Shen, J.; Liu, J.; Gao, Y.; Cao, D.; Zhang, L. Revisiting the Dispersion Mechanism of Grafted Nanoparticles in Polymer Matrix: A Detailed Molecular Dynamics Simulation. *Langmuir* **2011**, *27*, 15213−15222.
(36) Shi, R.; Qian, H.-J.; Lu, Z.-Y. Computer Simulation Study on the Self-Assembly of Unimodal and Bimodal Polymer-Grafted Nanoparticles in a Polymer Melt. *Phys. Chem. Chem. Phys.* **2017**, *19*, 16524−16532.
(37) Starr, F.; Douglas, J.; Glotzer, S. Origin of Particle Clustering in a Simulated Polymer Nanocomposite and its Impact on Rheology. *J. Chem. Phys.* **2003**, *119*, 1777−1788.
(38) Koski, J. P.; Ferrier, R. C., Jr; Krook, N. M.; Chao, H.; Composto, R. J.; Frischknecht, A. L.; Riggleman, R. A. Comparison of Field-Theoretic Approaches in Predicting Polymer Nanocomposite Phase Behavior. *Macromolecules* **2017**, *50*, 8797−8809.
(39) Liu, J.; Gao, Y.; Cao, D.; Zhang, L.; Guo, Z. Nanoparticle Dispersion and Aggregation in Polymer Nanocomposites: Insights From Molecular Dynamics Simulation. *Langmuir* **2011**, *27*, 7926−7933.
(40) Lin, Y.-L.; Chiou, C.-S.; Kumar, S. K.; Lin, J.-J.; Sheng, Y.-J.; Tsao, H.-K. Self-Assembled Superstructures of Polymer-Grafted Nanoparticles: Effects of Particle Shape and Matrix Polymer. *J. Phys. Chem. C* **2011**, *115*, 5566−5577.
(41) Martin, T. B.; Mongcopa, K. I. S.; Ashkar, R.; Butler, P.; Krishnamoorti, R.; Jayaraman, A. Wetting-Dewetting and Dispersion-Aggregation Transitions Are Distinct for Polymer Grafted Nanoparticles in Chemically Dissimilar Polymer Matrix. *J. Am. Chem. Soc.* **2015**, *137*, 10624−10631.
(42) Yethiraj, A. Entropic and Enthalpic Surface Segregation From Blends of Branched and Linear Polymers. *Phys. Rev. Lett.* **1995**, *74*, 2018.
(43) Humphrey, W.; Dalke, A.; Schulten, K. VMD − Visual Molecular Dynamics. *J. Mol. Graphics* **1996**, *14*, 33−38.
(44) Akcora, P.; Liu, H.; Kumar, S. K.; Moll, J.; Li, Y.; Benicewicz, B. C.; Schadler, L. S.; Acehan, D.; Panagiotopoulos, A. Z.; Pryamitsyn, V.; Ganesan, V.; Ilavsky, J.; Thiyagarajan, P.; Colby, R. H.; Douglas, J. F. Anisotropic Self-Assembly of Spherical Polymer-Grafted Nanoparticles. *Nat. Mater.* **2009**, *8*, 354−359.
(45) Hooper, J. B.; Schweizer, K. S. Theory of Phase Separation in Polymer Nanocomposites. *Macromolecules* **2006**, *39*, 5133−5142.
(46) Meng, D.; Kumar, S. K.; Cheng, S.; Grest, G. S. Simulating the Miscibility of Nanoparticles and Polymer Melts. *Soft Matter* **2013**, *9*, 5417−5427.
(47) Asakura, S.; Oosawa, F. On Interaction between Two Bodies Immersed in a Solution of Macromolecules. *J. Chem. Phys.* **1954**, *22*, 1255−1256.
(48) Asakura, S.; Oosawa, F. Interaction between Particles Suspended in Solutions of Macromolecules. *J. Polym. Sci.* **1958**, *33*, 183−192.
(49) Swain, A.; Begam, N.; Chandran, S.; Bobji, M.; Basu, J. Engineering Interfacial Entropic Effects to Generate Giant Viscosity Changes in Nanoparticle Embedded Polymer Thin Films. *Soft Matter* **2020**, *16*, 4065−4073.
(50) Das, N.; Begam, N.; Chandran, S.; Swain, A.; Sprung, M.; Basu, J. Thermal Stability and Dynamics of Soft Nanoparticle Membranes: Role of Entropy, Enthalpy and Membrane Compressibility. *Soft Matter* **2020**, *16*, 1117−1124.
(51) Meli, L.; Arceo, A.; Green, P. F. Control of the Entropic Interactions and Phase Behavior of Athermal Nanoparticle/Homopolymer Thin Film Mixtures. *Soft Matter* **2009**, *5*, 533−537.
(52) Green, P. F. The Structure of Chain End-Grafted Nanoparticle/Homopolymer Nanocomposites. *Soft Matter* **2011**, *7*, 7914−7926.
(53) Chen, X. C.; Green, P. F. Structure of Thin Film Polymer/Nanoparticle Systems: Polystyrene (PS) Coated-Au Nanoparticle/Tetramethyl Bisphenol-A Polycarbonate Mixtures (TMPC). *Soft Matter* **2011**, *7*, 1192−1198.
(54) Corbierre, M. K.; Cameron, N. S.; Sutton, M.; Laaziri, K.; Lennox, R. B. Gold Nanoparticle/Polymer Nanocomposites: Dispersion of Nanoparticles as a Function of Capping Agent Molecular Weight and Grafting Density. *Langmuir* **2005**, *21*, 6063−6072.
(55) Chevigny, C.; Dalmas, F.; Di Cola, E.; Gigmes, D.; Bertin, D.; Boué, F.; Jestin, J. Polymer-Grafted-Nanoparticles Nanocomposites: Dispersion, Grafted Chain Conformation, and Rheological Behavior. *Macromolecules* **2011**, *44*, 122−133.
(56) Kremer, K.; Grest, G. S. Dynamics of Entangled Linear Polymer Melts: A Molecular-Dynamics Simulation. *J. Chem. Phys.* **1990**, *92*, 5057−5086.
(57) Plimpton, S. Fast Parallel Algorithms for Short-Range Molecular Dynamics. *J. Comput. Phys.* **1995**, *117*, 1−19.
(58) Auhl, R.; Everaers, R.; Grest, G. S.; Kremer, K.; Plimpton, S. J. Equilibration of Long Chain Polymer Melts in Computer Simulations. *J. Chem. Phys.* **2003**, *119*, 12718−12728.
(59) Hsu, H.-P.; Kremer, K. Static and Dynamic Properties of Large Polymer Melts in Equilibrium. *J. Chem. Phys.* **2016**, *144*, 154907.
(60) Grest, G. S. Communication: Polymer Entanglement Dynamics: Role of Attractive Interactions. *J. Chem. Phys.* **2016**, *145*, 141101.

https://dx.doi.org/10.1021/acsnano.0c05495
ACS Nano 2020, 14, 13491−13499